A COMMERCIAL CPT RUBIDIUM CLOCK

Jinquan Deng, Peter Vlitas, Dwayne Taylor, Larry Perletz, and Robert Lutwak

Symmetricom Inc, Beverly, MA 01915, USA

Abstract

This paper shows a miniature commercial atomic clock – SA.3Xm, based on coherent population trapping (CPT). We present the architecture of the CPT clock, including fundmental laser requirements, physical characteristics, and servo architecture. The general clock performance, including short-term frequency stability, temperature coefficient, frequency retrace, and frequency aging, is shown.

1. Introduction

Microwave atomic frequency standards use resonances within atoms to keep precise frequency and time. The natural atomic resonances are intrinsically more stable and less sensitive to environmental perturbations, such as temperature, pressure, humidity, vibration, and acceleration, than are macroscopic oscillators such as pendulums and quartz crystals. The atomic resonator is used as a highly stable frequency reference to which a variable frequency oscillator, such as a quartz oscillator, is locked, thereby imparting the high stability and environmental insensitivity of the atoms to the output signal. All commercially-available atomic clocks exploit ground-state microwave hyperfine transition frequencies of atoms in an atomic gas or beam. Generally, state selection is accomplished by either magnetic spatial deflection or optical pumping, and the resonance frequency is detected by the classical magnetic resonance technique.

Coherent population trapping (CPT), accomplished by means of a laser radiation field with two wavelengths applied in a so-called Λ scheme [1], provides an alternative to the classic approach. CPT makes possible the simultaneous preparation and resonance excitation of the atomic ensemble in the same region of space. In the case of alkali atoms, the fields are applied to an ensemble of atoms in resonance with the transitions between the two hyperfine levels of the $S_{1/2}$ ground state and one of the P-state hyperfine levels, forming the Λ scheme. Due to off-diagonal coherent excitation, an interference appears in the excitation process, coherence is created in the ground state, and the ensemble of atoms is placed in a non-absorbing state called a 'dark' state. The phenomenon, as observed at a hyperfine frequency, was reported for the first time by Alzetta et al. in sodium atoms using a multimode dye laser [1].

The first effort to create a CPT atomic clock was reported by Thomas et al [2]. In those experiments, a Ramsey-type separated fields interrogation was performed on a beam of sodium sodium atoms, entirely with light beams and without the classical Ramsey microwave cavity. With the development of suitable solid-state lasers, in the1990s, it became practical to implement small-scale atomic frequency standards based on the application of the CPT phenomenon in sealed vapor cells. In 1993 Cyr et al. [3] proposed a simple method to observe a ^{87}Rb microwave clock transition by purely optical means using a laser modulated at a sub-harmonic of hyperfine frequency of the ground state of ^{87}Rb. Liu et al. [4] demonstrated Raman polarization-selective feedback schemes for all-optical microwave frequency standards in 1996. Levi et al. [5] presented preliminary experimental results on a passive CPT clock with fluorescence detection and an excitation laser modulated at half the hyperfine splitting frequency. Brandt et al. [6] reported a narrow CPT resonance with linewidth of 42 Hz. Kernco Inc [7] reported an industrial implementation of a CPT passive frequency standard using ^{87}Rb. Most recently, the CPT phenomenon has been used in the realization of chip-scale atomic clocks (CSAC) [8–10].

At Symmetricom, CPT research has been ongoing since the mid-1990s. The productization of a fieldable, robust atomic clock based on CPT technology has been hindered to date by the lack of suitably performing and reliable cost-effective laser sources. This has evolved, in recent years, with the introduction of single-transverse-mode (STM) vertical cavity surface emitting lasers (VCSELs), which can be customized to provide nearly ideal properties for CPT interrogation. We have recently completed development of Symmetricom's first atomic clock product employing CPT technology, the SA.3Xm. The SA.3Xm, which utilizes CPT interrogation of the ^{87}Rb D_1 resonance line, provides performance comparable to that of conventional rubidium oscillators with reduced cost, volume, and power consumption.

This paper presents the architecture of the SA.3Xm, including fundmental laser requirements, physical characteristics, and both light and microwave controls. The general clock performance, including short-term frequency stability, temperature coefficient, frequency retrace, and frequency aging, will be presented.

2. CPT

A. Experimental Setup

Coherent population trapping in atomic rubidium may be observed by a simple scheme as shown in Fig. 1. The laser source is a 795 nm VCSEL, which operates in both single longitude mode and single transverse mode, in a constant polarization orientation. The VCSEL is mounted on a thermoelectric cooler (TEC) for temperature control.

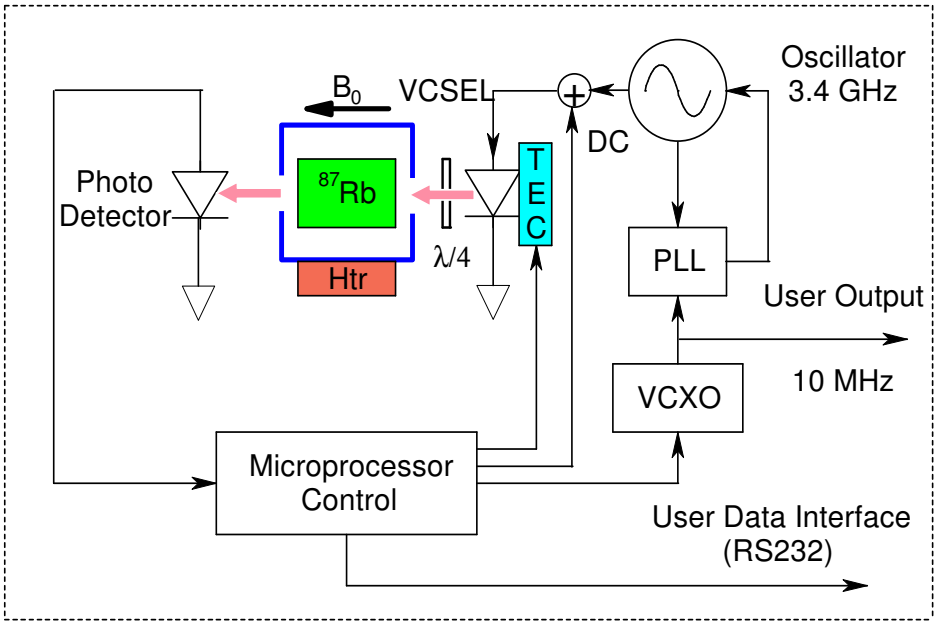

Figure 1. Experimental setup for observing CPT resonance and building a CPT clock.

In order to produce the coherent sidebands necessary for CPT interrogation, the VCSEL's current is modulated at half the hyperfine frequency, 6.834GHz/2 = 3.417 GHz. This produces sidebands in the laser spectrum. The first two sidebands are separated by twice the modulated frequency and are used as the two CPT radiation fields. The λ/4 plate, in Fig. 1, provides circular polarization as required by the selection rules for the excitation process. B_0 is the applied magnetic field which provides an axis of quantization for the atomic ensemble. The resonance cell contains ^{87}Rb and a small amount of buffer gas which increases the transit time of atoms across the laser beam and reduces collisions between rubidium atoms and between rubidium atoms and the cell walls, both of which adversely impact the lifetime of the coherent state. The photodetector detects the transmitted CPT resonance signal.

Microwaves at $\nu_{0\text{-}0}/2$ = 3.4 GHz are synthesized from a 10.0 MHz VCXO as shown on the right of Fig. 1. In order to implement a CPT clock, the microwave frequency is locked to the CPT signal from the resonance cell, thereby stabilizing the output frequency at 10.0 MHz. A serial output from the microprocessor provides a control and data interface.

B. Optical Absorption Spectrum

The optical absorption spectrum of the modulated laser radiation, shown in Fig. 2, is a complex convolution of the laser spectrum and the four main absorption lines of the ^{87}Rb D1 resonance. The hyperfine structure of the excited state is not resolved in the optical absorption spectrum.

The shape of this spectrum is very sensitive to the amplitude of the applied microwave power, typically

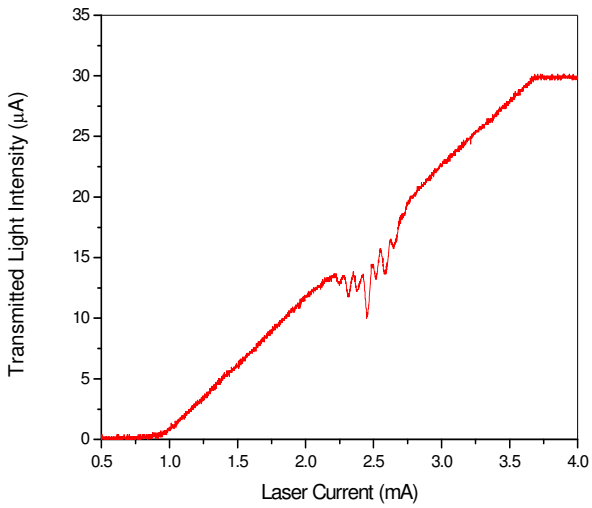

Figure 2. Experimental optical absorption spectrum for a frequency modulated VCSEL .

quantified by the modulation index. The first two sidebands of the modulated laser spectrum have the highest amplitude when the modulation index is 1.8, which gives the strongest CPT resonance signal. When the modulation index is 2.4, where the carrier amplitude is zero, the CPT clock has the smallest light shift effect [11].

C. CPT Resonance

After the laser wavelength is locked to the deepest resonance of Fig. 2, we sweep the microwave frequency around 3.417 GHz. The change in the dc transmitted light intensity is monitored by the photodetector. A plot of the photodetector signal with the detuning frequency is shown in Fig. 3.

The CPT resonance in Fig. 3 has a contrast of ~1.6%, and a linewidth of ~300 Hz. This gives a figure-of-merit ($1x10^6$ Hz•contrast/linewidth) of 53. This predicts a corresponding clock short-term Allan deviation frequency stability of less than $3x10^{-11}$ at 1 second for a typical clock-usable VCSEL.

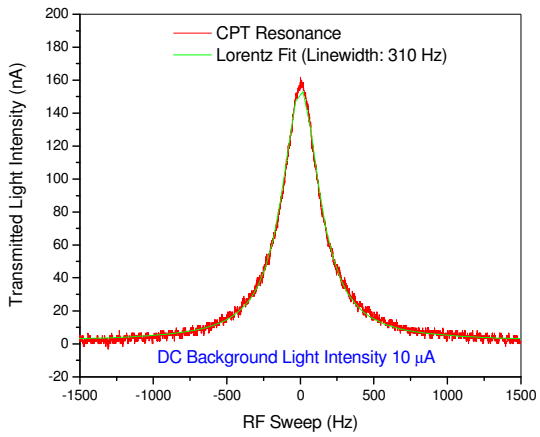

Figure 3. CPT resonance from SA.3Xm ^{87}Rb cell, Red-data, Green-Lorentzian Fit.

D. Light Intensity and Microwave Modulation Index Control

The laser wavelength is stabilized to the optical absorption resonance in the Rb resonance cell, but its intensity may change with time due to both intensity and wavelength aging of the VCSEL. Therefore the clock frequency also changes because of the light shift effect. Deng et al. [12] proposed a method to control both the laser wavelength and intensity simultaneously. In this method, the laser wavelength is controlled by the laser injection current (fast servo loop), and the light intensity is stabilized by controlling the laser temperature (slow servo loop). Operating simultaneously, the two control loops maintain both the temperature and the injection current of the VCSEL such that the light intensity is held constant (to minimize light shift effects) and the laser wavelength remains locked to the atomic resonance.

When the microwave power varies, it also causes a light shift to the clock frequency due to the change of the modulation index and, thereby, the laser spectrum. This can lead to both short- and long-term instability of the clock frequency. In the Sa.3X.m, the microwave power is continuously servo controlled to the atomic signal in order to provide optimal and stable interrogation conditions.

3. SA.3Xm

The SA.3Xm is Symmetricom's first commercial product based on CPT interrogation. This necessitated the research and development of new electronic and mechanical architectures and control systems, as well as the development of manufacturing technologies. Nonetheless, development of the SA.3Xm at Symmetricom took less than 24 months, from initial concept to production release. We have recently completed a pilot production build.

A. SA.3Xm Photos

A photograph of SA.3Xm is shown in Figs. 4 (a) (outside) and 4 (b) (inside). The physical dimension is 5.1 cm by 5.1 cm by 1.8 cm, with a total volume of about 47 cc. It has the same footprint and pinout as a typical 5.1 cm by 5.1 cm ovenized quartz oscillator.

(a)

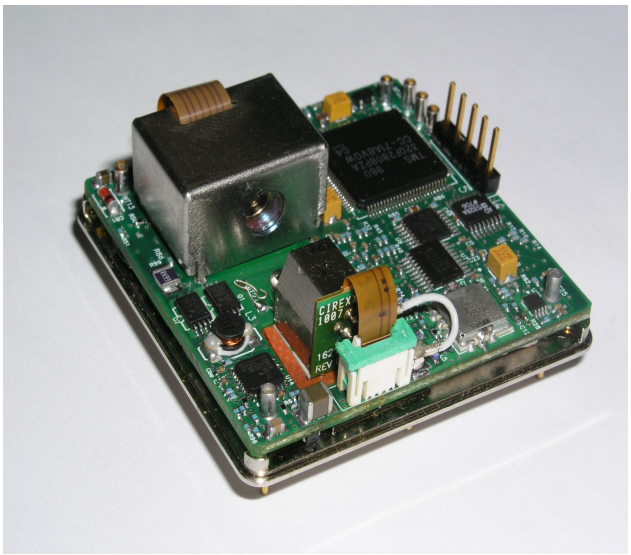

(b)

Figure 4. Symmetricom CPT clock SA.3Xm.

The principal components of the SA.3Xm are shown in Fig. 4b, with the cover removed. The resonance cell (top left) is temperature-stabilized and contained within a two-layer high-permeability magnetic shield. The VCSEL (lower left) is mounted atop a thermoelectric cooler for precise and independent temperature control. The

microprocessor (top right) manages initial acquisition and continuous optimization of the servo loops. The microprocessor also provides RS-232 communications with the host system for status monitoring and digital calibration.

B. Short-term Stability

Fig. 5 shows typical short-term frequency stability of the SA.3Xm. The Allan deviation frequency stability shown below is $<3x10^{-11}\,\tau^{-1/2}$ for $\tau < 20$ s, and $<5x10^{-11}\,\tau^{-1/2}$ for $\tau < 2{,}000$ s.

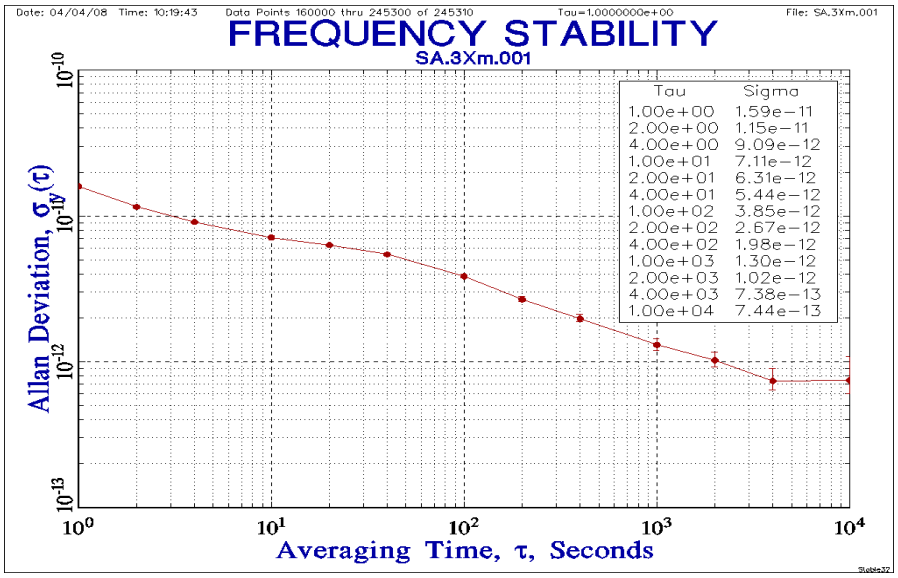

Figure 5. Typical SA.3Xm short-term frequency stability.

C. Temperature Coefficient and Compensation

To evaluate the performance of the SA.3X.m, the unit was installed in a temperature-controlled chamber. The left side of Fig. 6 (up to MJD 54525.8) shows the frequency offset of SA.3Xm (top plot in green) as the chamber temperature (bottom plot in red) was varied in 10 °C steps from –20 to 65 °C, with one and a half hour dwell at each temperature. The total frequency change corresponding to this temperature change is approximately $\Delta y = -3.4x10^{-10}$.

We are able to improve the temperature performance considerably by employing digital compensation, via an onboard temperature sensor and microprocessor control of the microwave synthesizer. The temperature compensated frequency performance is shown on the right side of Fig. 6. In this evaluation, the chamber temperature was ramped linearly from –20 to 65° C over 6 hours. With compensation enabled, the observed frequency change was less than $3x10^{-11}$, an improvement of one order of magnitude over the uncompensated performance.

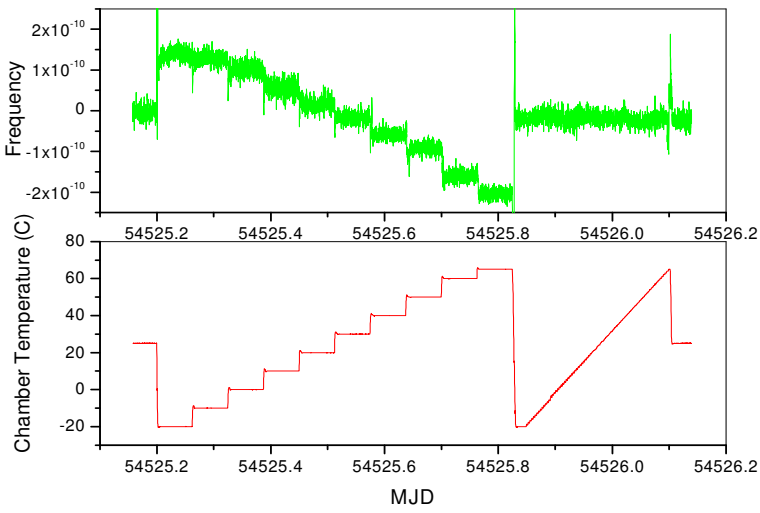

Figure 6. Uncompensated and compensated SA.3Xm temperature performance.

D. Frequency Retrace

Retrace is defined as frequency reproducibility upon power-cycling the unit. In our laboratory, we measure retrace by periodically cycling power to the unit while monitoring the frequency output. Fig. 7 shows a typical retrace measurement. The beginning part of Fig. 7 was cycled with a 1-hour on/3-hour off duty cycle. The end part was cycled with a 3-hour on/1-hour off duty cycle. Each test lasted approximately 3 days. The retrace is less than $1x10^{-11}$. The visible frequency fluctuation of $2x10^{-11}$ is due to ambient temperature fluctuations.

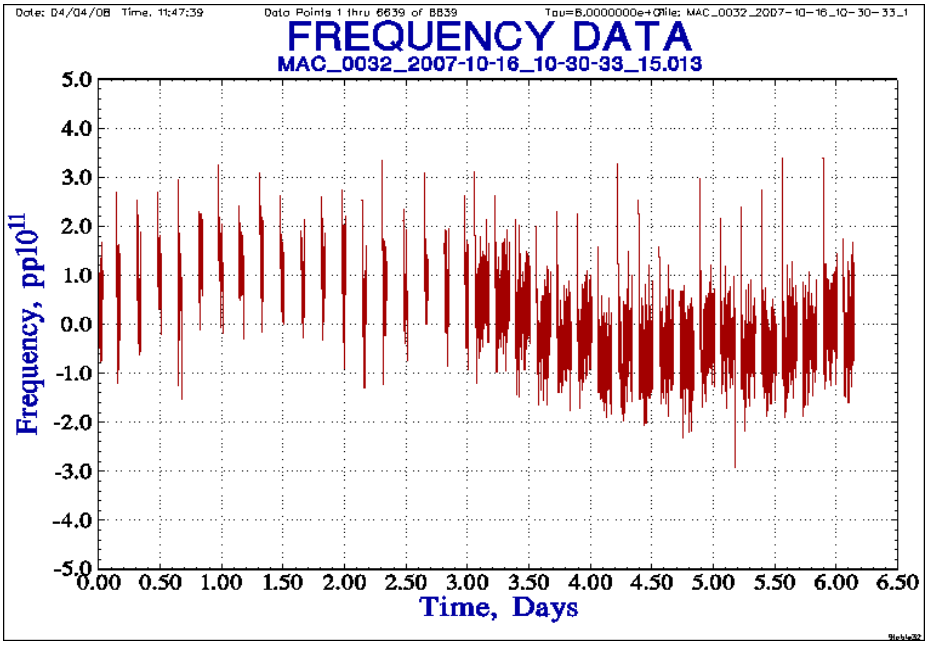

Figure 7. Clock frequency retrace of SA.3Xm.

E. Frequency Aging

We have monitored the long-term frequency behavior of several SA.3Xm oscillators for approximately 170 days. Typical long-term frequency performance is shown in Fig. 8. The exponentially-decaying-positive-aging is typical of the many units we have evaluated. Initially, the aging is fairly large (≈$1x10^{-11}$/day) for the first few days. Over the first month of operation, the aging decreases to approximately $1x10^{-10}$/month. Following 75 days of equilibration, the aging reaches $5x10^{-11}$/month, which is a typical specification for conventional rubidium oscillators.

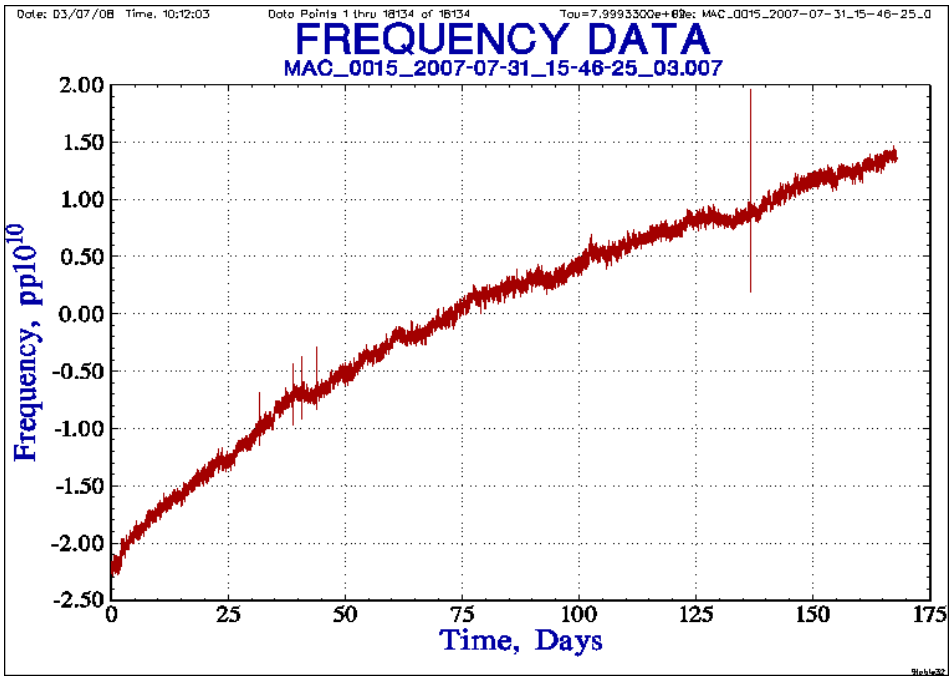

Figure 8. Long-term aging of SA.3Xm

G. Data From Pilot Build

In our pilot production build, we have evaluated performance including Allan deviation frequency stability, phase noise, and temperature coefficient.

Fig. 9 shows a histogram of the 10s frequency stability in Red, Gaussian fit in Green, and the specification in Blue. The mean is ~1x10^{-11} and the standard deviation is ~2.5 x10^{-12}.

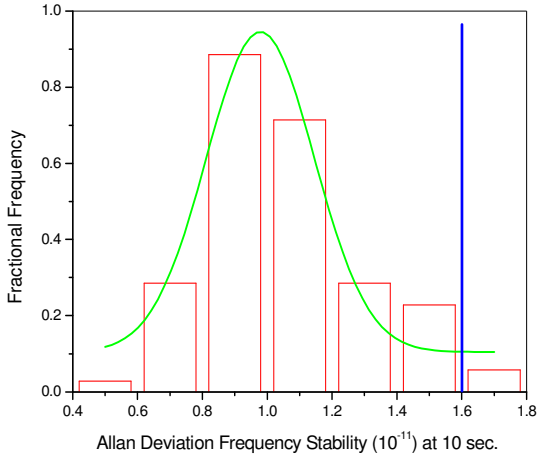

Figure 9. Histogram of 10 s Frequency Stability.

As mentioned above, we measure temperature performance of the units in a chamber. A histogram of temperature coefficient before and after the digital temperature compensation is shown Fig. 10. The mean temperature coefficients are 3.5 x10^{-10} and 4.3 x10^{-11}, respectively. All of the temperature coefficients meet our specification (in Blue of Fig. 10) with a 20% margin. From our experience, this is an excellent result compared with traditional Rb oscillators.

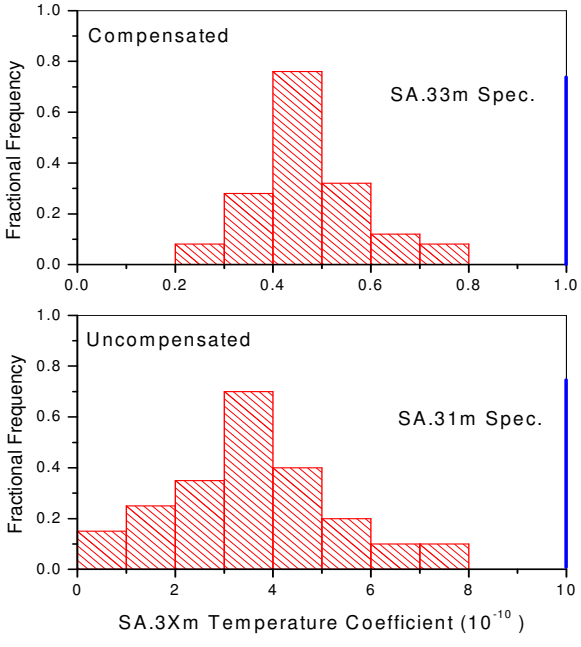

Figure 10. Histogram of Temperature Coefficient.

The histogram of the phase noise on the 10 MHz output is shown in Fig. 11 and in Table 1. At 1 Hz and 10 Hz from the carrier, where the phase noise is determined by the properties of the atomic resonance rather than by those of the quartz oscillator, approximately 5% of the units missed the specification (in Blue of Fig. 11). Improvement of the performance in this regime is an area of active investigation.

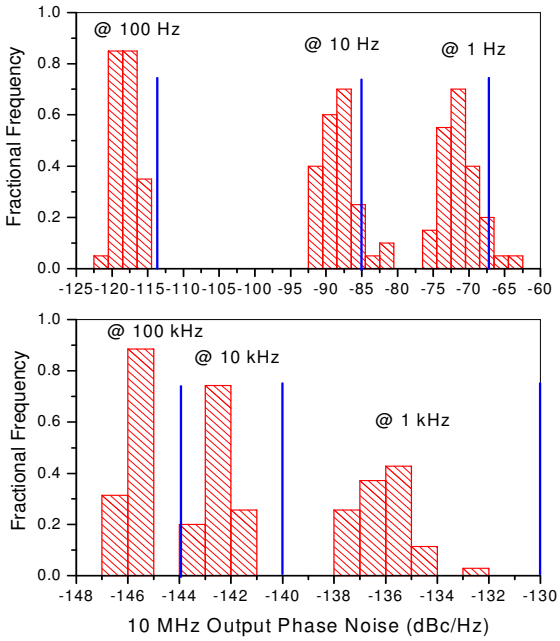

Figure 11. Histogram of Phase Noise.

Table 1. SA.3X.m's phase noise specification and measured mean with standard deviation.

Frequency From Carrier	**1** (Hz)	**10** (Hz)	**100** (Hz)	**1** (kHz)	**10** (kHz)	**100** (kHz)
Spec. (dBc/Hz)	-67	-85	-114	-130	-140	-144
Measured Mean	-71	-88	-118	-136	-143	-146
Standard Deviation	2.6	2.4	1.3	1.1	0.6	0.3

4. Conclusion

Based on the CPT method of interrogation, we have developed a miniature commercial atomic clock, the SA.3Xm. It is about one-third the size and consumes less than half the power compared to conventional Rb oscillators. SA.3Xm exhibits excellent temperature coefficient of <1x10^{-10} and retrace of <2x10^{-11}. Its Allan deviation frequency stability is <3x10^{-11} $\tau^{-1/2}$ for τ <20 s, and <5x10^{-11} $\tau^{-1/2}$ for τ<2,000 s, which is compatible to the existing commercial Rb oscillators. The data analysis of the pilot production build units shows good reproducibility. The SA.3Xm is ideal for a wide variety of applications, such as mobile base stations, transmission stations, network elements, and other communications equipment.

Acknowledgment

The authors thank M. Silveira, A Rashed for assistance in testing, M. Garvey, D. Emmons, and J. Dansereau for helpful discussions and project management.

Reference

[1] G. Alzetta, A. Gozzini, M. Moi, G. Orriols, Nuovo Cimento B **36**, 5(1976).

[2] J.E. Thomas, P.R. Hemmer, S. Ezekiel, C.C. Leiby, H. Picard, and R.Willis, Phys. Rev. Lett. **48**, 867 (1982).

[3] N. Cyr, M. Tetu, M. Breton, IEEE Trans. Instrum. Meas. **42**, 640 (1993).

[4] Z.D.Liu, P. Juncar, D. Bloch, and M. Ducloy, Appl. Phys. Lett. **69**(16), 2318 (1996).

[5] F. Levi, A. Godone, C. Novero, and J. Vanier, in *Proceedings of the 11th European Frequency and Time Forum*, 216 (1997).

[6]. S. Brandt, A. Nagel, R. Wynands, and D. Meschede: Phys. Rev. A **56**, R1063 (1997).

[7] J. Vanier, M. Levine, S. Kendig, D. Janssen, C. Everson, and M. Delaney, in *Proceedings of the IEEE International Ultrasonics, Ferroelectrics, and Frequency Control Joint 50th Anniversary Conference*, 92 (2004).

[8] R. Lutwak, D. Emmons, T. English, W. Riley, A. Duwel, M. Varghese, D.K. Serkland, and G.M. Peake, in *Proceedings of the 35th Precise Time and Time Interval (PTTI) Systems and Applications Meeting*, 1 (2003).

[9] M. Zhu, L.S. Cutler, J.E. Berberian, J.F. Denatale, P.A. Stupar, and C. Tsai, in *Proceedings of the IEEE International Ultrasonics, Ferroelectrics, and Frequency Control Joint 50th Anniversary Conference*, Montr´eal, 100 (2004).

[10] S. Knappe, L.-A. Liew, P. Swchwind, V. Shah, J.Moreland, L. Hollberg, and J. Kitching, in *Proceedings of the IEEE International Ultrasonics, Ferroelectrics, and Frequency Control Joint 50th Anniversary Conference*, Montr´eal, 87 (2004).

[11] M. Zhu, and L.S. Cutler, in *Proceedings of the 32nd Precise Time and Time Interval (PTTI) Systems and Applications Meeting*, 311 (2000).

[12] J.Q. Deng, J. D. Crockett, and T. C. English, US Patent, 6,927,636 B2, (2005).